Exploring shape (phase) evolution in even-even $^{126-136}$Ba*

Jie Yang (杨婕)[1] Xin Guan (关鑫)[1†] Rong-Xin Nie (聂荣鑫)[1] Hua-Lei Wang (王华磊)[2‡]
Feng Pan (潘峰)[1,2] Jerry P. Draayer[3]

[1]School of Physics and Electronic Technology, Liaoning Normal University, Dalian 116029, China
[2]School of Physics, Zhengzhou University, Zhengzhou 450001, China
[3]Department of Physics and Astronomy, Louisiana State University, Baton Rouge, LA 70803-4001, USA

Abstract: In this study, the evolution of nuclear shape and rotational behavior along the yrast line in even-even $^{126-136}$Ba was systematically investigated using pairing self-consistent Woods-Saxon-Strutinsky calculations combined with the total Routhian surface (TRS) method in the (β_2,γ,β_4) deformation space. Empirical laws were applied to evaluate nuclear ground-state properties, revealing a shape evolution from axially deformed to non-axial vibrational configuration in even-even $^{126-136}$Ba isotopes. Particularly, an extreme γ-unstable shape was predicted in ^{130}Ba. The shape transition of the ground state in these nuclei was confirmed by the TRS calculations. In addition, the evolution of the nuclear shape in high spin states with varying rotational axes associated with rotation around the medium, long, and short axes was elucidated from the TRS calculations. This variation was further characterized by the alignment of the $\pi(h_{11/2})^2$ and $\nu(h_{11/2})^2$ configurations, highlighting a preference for non-collective oblate/triaxial shapes with $\gamma > 0°$ and collective oblate/triaxial shapes with $\gamma < 0°$, respectively.

Keywords: total-Routhian-surface calculations, cranked shell model, empirical laws, rotation alignment, nuclear structure

DOI: 10.1088/1674-1137/adc2da **CSTR:** 32044.14.ChinesePhysicsC.49074104

I. INTRODUCTION

The nuclear structure at high spin is typically described by a semiclassical model of a rotating average field in which an intrinsic shape rotates uniformly around a fixed spatial axis, representing rotation as a specific collective motion in finite many-body systems [1]. The physical consequences of such motion are influenced by shape asymmetry characterized by the lowest order of quadrupole and triaxial deformations, which affect the time dependence of the nuclear and Coulomb fields [2, 3]. Most deformed nuclei exhibit axial symmetry in their ground states, whether oblate or prolate, allowing collective rotation only around the perpendicular axis. However, some nuclei have been observed to have triaxial ground-state deformations, as indicated by nuclear mass analyses [4]. In particular, nuclei in the $A \approx 130$ mass region are known to exhibit axial asymmetry in their ground states [5]. In this region, the proton Fermi surface lies in the lower part of the $h_{11/2}$ orbitals, favoring a prolate shape, while neutrons occupy medium-to-high Ω orbitals in the same shell, potentially driving the shape toward an oblate configuration [6]. The competition between these opposing tendencies can result in a shape resembling a triaxial ellipsoid.

In a triaxially deformed potential, particles and holes tend to align their angular momenta along the short and long axes, respectively. According to the hydrodynamical model of rotation [3], the moment of inertia along the medium axis is the largest, favoring collective rotation around this axis. Consequently, the total angular momentum vector has nonzero components along all three principal axes [7]. For a triaxial nucleus, rotation can occur around any of the three principal axes. Principal-axis cranking calculations reveal that rotation can indeed take place around any of these axes, corresponding to three different minima in the total energy surface within the (β_2,γ) plane [8]. However, the rotational axis of a triaxial nucleus typically coincides with the principal axis that has the largest moment of inertia, leading to the lowest-energy (yrast) states.

Throughout the yrast states, transitions can occur between rotations characterized by varying relationships between aligned angular momentum and rotational frequency. Aligned quasiparticles influence the nuclear

Received 6 February 2025; Accepted 19 March 2025; Published online 20 March 2025
* Supported by the National Natural Science Foundation of China (12275115, 11975209, 12175097), and Natural Science Foundation of Henan (252300421478)
† E-mail: guanxin@lnnu.edu.cn
‡ E-mail: wanghualei@zzu.edu.cn

shape and subsequent alignments. Even-even $^{126-136}$Ba belong to a transitional region [9] in which nuclear structure characteristics have been extensively studied using various models. The presence of two *S*-bands in this mass region is commonly attributed to the shape-driving effects of aligned $h_{11/2}$ neutrons and protons acting on relatively soft nuclear cores [6]. Theoretical approaches, such as microscopic models [9], interacting boson model (IBM) [10], and general collective model (GCM) [11], have also been extensively used to study the low-energy spectrum in this region. The cranking approximation for the covariant density function theory was used to study the global dynamical correlation energies for the nuclei from $Z = 8$ to $Z = 108$ [12−16]. Recently, the cranking covariant density functional theory in a three-dimensional lattice space has been employed to investigate the octuple magic nucleus ^{144}Ba [17]. Despite some experimental data and theoretical models addressing this phenomenon, a comprehensive and systematic study, especially regarding the stability and mechanisms of shape evolution at high spins, is still lacking. Therefore, it is necessary to adopt appropriate nuclear models to study both the ground state and high-spin shape evolution in Ba isotopes for a deeper understanding of their structural properties.

In previous studies of ours, we investigated the evolution of ground-state quadrupole and octupole stiffnesses in even-even $^{112-150}$Ba using potential energy surface (PES) calculations [18]. We noticed that $^{118-128}$Ba has more stable quadrupole deformations and we reproduced their experimental properties using total Routhian surface (TRS) calculations [19]. In addition, $^{126-136}$Ba showed a dramatic increase with respect to the non-axial γ deformation [18]. According to these findings, it is meaningful to continue studying the shape evolution in these isotopes, particularly focusing on the stability of shape variations in high-spin states.

In this study, the nuclear shape evolution and rotational behavior along the yrast line in even-even $^{126-136}$Ba isotopes were investigated using TRS calculations in the (β_2,γ,β_4) deformation space. Our results reveal a transition from axially deformed shapes to non-axial configurations, with extreme γ-unstable shapes predicted for ^{130}Ba. We also explored the evolution of the nuclear shape in high-spin states, showing a preference for non-collective oblate/triaxial shapes for $\gamma > 0°$ and collective oblate/triaxial shapes for $\gamma < 0°$.

II. THEORETICAL FRAMEWORK

The TRS calculations applied here are based on the pairing-deformation self-consistent cranked shell model (CSM) [20−22]. This approach generally provides a reliable description of high-spin phenomena in rapidly rotating medium and heavy mass nuclei. The total Routhian, referred to as "Routhian" rather than "energy" in the rotating frame of reference, represents the sum of the energy of the ground state and the contribution from cranking.

The energy of the ground state is composed of a macroscopic component and a fluctuating microscopic component. The macroscopic part is derived from the standard liquid-drop model (LDM) with parameters established by Myers and Swiatecki [23]. The microscopic correction, arising from the non-uniform distribution of single-particle levels in the nucleus, mainly includes a shell correction and a pairing correction, calculated using the Strutinsky [24] and Lipkin-Nogami (LN) [25] methods, respectively. The Strutinsky smoothing procedure employs a sixth-order Laguerre polynomial with a smoothing range of 1.20 $\hbar\omega_0$, where $\hbar\omega_0 = 41/A^{1/3}$ MeV. The LN method is used to avoid the spurious pairing phase transitions encountered in simpler Bardeen-Cooper-Schrieffer (BCS) calculations. Both the shell and pairing corrections are evaluated based on a set of single-particle energy levels.

The single-particle energies required for the shell correction are obtained from the non-axially deformed Woods-Saxon (WS) potential, using a parameter set commonly employed in cranking calculations [26]. During the diagonalization of the WS Hamiltonian, oscillator basis states with principal quantum numbers $N \le 12$ for protons and $N \le 14$ for neutrons have been used. The nuclear shape is defined using the standard parametrization expanded in spherical harmonics [26]. The nuclear surface radius, $R(\theta,\phi)$, extending from the origin to the surface of the nucleus, is described by the expression provided in [1]:

$$R(\theta,\phi) = R_0\, c(\hat{\beta})\Big[1 + \sum_{\lambda=1}^{\infty}\sum_{\mu=-\lambda}^{\lambda}\alpha_{\lambda\mu}Y^*_{\lambda\mu}(\theta,\phi)\Big]. \tag{1}$$

R_0 represents the radius at spherical equilibrium with the same volume, $R_0 = r_0A^{1/3}$; the function $c(\hat{\beta})$ ensures the conservation of the nuclear volume with a change in the nuclear shape; $\hat{\beta}$ denotes the set of all the deformation parameters; and $\alpha_{\lambda\mu}$ denotes the shape parameters. In general, a limit expressed as $\lambda < A^{1/3}$ can be obtained by a crude estimate [27]. The nuclear surface is described, for our purposes, by a second-order deformation [28].

In the present shape parametrization, we consider quadrupole and hexadecapole degrees of freedom, including nonaxial deformations, defined as $\hat{\beta} \equiv (\alpha_{20},\alpha_{2\pm2},\alpha_{40},\alpha_{4\pm2},\alpha_{4\pm4})$. Assuming the existence of three symmetry planes–(x,y), (y,z), and (x,z)–the number of independent coefficients α is reduced to five. These are expressed as

$$\alpha_{22} = \alpha_{2-2}, \qquad \alpha_{42} = \alpha_{4-2}, \qquad \alpha_{44} = \alpha_{4-4}, \tag{2}$$

where α_{20} and α_{40} can be expressed in terms of the standard (β_2,γ,β_4) parameters as

$$\begin{cases} \alpha_{20} = \beta_2\cos\gamma \\ \alpha_{22} = \alpha_{2-2} = \dfrac{1}{\sqrt{2}}\beta_2\sin\gamma \\ \alpha_{40} = \dfrac{1}{6}\beta_4(5\cos^2\gamma+1) \\ \alpha_{42} = \alpha_{4-2} = \dfrac{1}{12}\sqrt{30}\beta_4\sin 2\gamma \\ \alpha_{44} = \alpha_{4-4} = \dfrac{1}{12}\sqrt{70}\beta_4\sin^2\gamma. \end{cases} \tag{3}$$

This leads to a three-dimensional problem with the usual (β_2,γ,β_4) degrees of freedom. The quadrupole deformation parameter β_2 represents the magnitude of the deformation whereas the triaxiality parameter γ describes the deviation from axial symmetry.

Under the Lund convention [2], the Cartesian quadrupole coordinates were used to vary the quadrupole deformation in the calculations, including the γ degrees of freedom,

$$X = \beta_2\cos(\gamma+30^\circ) \qquad Y = \beta_2\sin(\gamma+30^\circ). \tag{4}$$

The γ parameter covers the range from -120° to 60°. This range can generally be divided into three sectors, namely $(-120^\circ<\gamma<-60^\circ)$, $(-60^\circ<\gamma<0^\circ)$, and $(0^\circ<\gamma<60^\circ)$, which represent the same triaxial shapes at the ground state but correspond to rotation about the long, medium, and short axes, respectively, at nonzero cranking frequency. The four limiting cases ($\gamma=-120^\circ,-60^\circ,0^\circ$, and 60°) correspond to the possible rotations of axially symmetric shapes: $\gamma=-120^\circ$ and 0° for prolate shapes and $\pm60^\circ$ for oblate shapes. These orientations describe different modes of rotation: $\gamma=-120^\circ$ and 60° indicate non-collective rotation around the symmetry axis, while $\gamma=-60^\circ$ and 0° correspond to collective rotation around an axis perpendicular to the symmetry axis.

Cranking constrains the nuclear system to rotate around a fixed axis (the x-axis) with a specified rotational frequency. Pairing correlations depend on both the rotational frequency and nuclear deformation. The resulting cranked-Lipkin-Nogami equation takes the form of the well-known Hartree-Fock-Bogolyubov-like (HFB) equation [22]. For a given rotational frequency and deformation point on the lattice, pairing correlations are treated self-consistently by solving this equation within a sufficiently large space of Woods-Saxon single-particle states.

The symmetries of the rotating potential can be used to simplify the cranking equations. In the reflection-symmetric case, both the signature quantum number r and intrinsic parity π remain proper quantum numbers. The solution characterized by (π,r) provides the energy eigenvalue, from which the energy relative to the non-rotating state can be directly obtained. After calculating the Routhians at fixed rotational frequencies, the values are interpolated using a cubic spline function between lattice points. The equilibrium deformation is then determined by minimizing the TRS.

III. RESULTS AND DISCUSSIONS

In nuclear structure research, phenomenological or empirical laws are often used as order parameters to reveal the shape phase evolution in nuclei [29]. Several such quantities and their evolution with the neutron number are represented in Fig. 1. The energy of the first $E(2_1^+)$ state serves as an indicator of the quadrupole deformation β_2 in terms of the general empirical relation $6\hbar^2/2J = E(2_1^+) \approx 1225/A^{7/3}\beta_2^2$ MeV [30, 31]. As shown in Fig. 1 (a), the energy of the 2_1^+ state increases as the neutron number approaches the $N=82$ closed shell, which indicates the decreasing of the nuclear quadrupole deformation β_2 with neutron far from the close shell number. In addition to the $E(2_1^+)$ states, the $B(E2)$ transitions from the first 2^+ to the ground state 0^+ are a powerful tool for studying the nuclear deformations following the approximation $B(E2:2^+)\rightarrow 0^+) \propto \beta_2^2$ [3]. As shown in Graph 28 of Ref. [32], the behavior of $B(E2:2^+)$ is inversely related to that of $E(2_1^+)$, as depicted in Fig. 1. As the number approaches shell closure, the $B(E2:2^+)$ transitions decrease, indicating a reduction in the prolate deformation.

Deviation of the nuclear shape from axial symmetry can significantly influence the second-lowest 2_2^+ state,

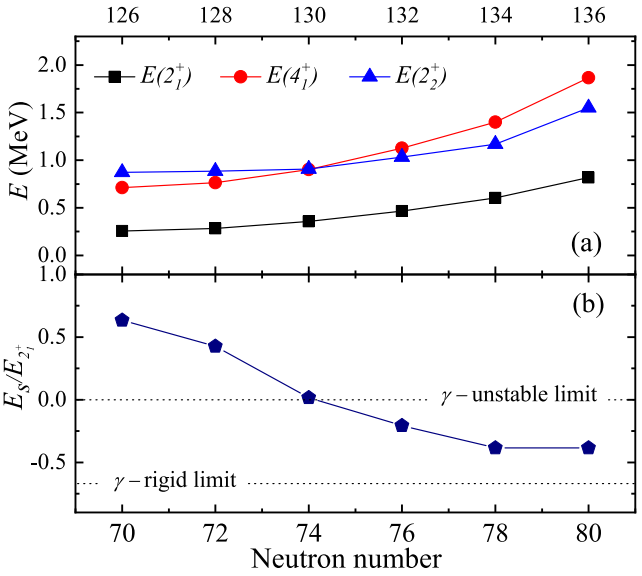

Fig. 1. (color online) (a) Energies of the first excited 2_1^+, 4_1^+, and 2_2^+ states, (b) energy ratio E_S/E_2^+.

commonly associated with the quasi-γ bandhead in even-even nuclei. As shown in Fig. 1 (b), systematic variation in the relative position of this 2_2^+ state with respect to the ground-state band can be clearly observed.

Empirically, the ratio $E_s/E(2_1^+)$, where $E_s = E(2_2^+) - E(4_1^+)$, plays the role of a global indicator of structural evolution associated with axial asymmetry [33]. In the extreme γ-unstable limit [34], the 2_2^+ and 4_1^+ states are completely degenerate, resulting in $E_s/E(2_1^+) = 0$, as observed in ^{130}Ba nuclei [5]. Conversely, for a rigid triaxial rotor with $25° \leq \gamma \leq 30°$ [35], the 2_2^+ state lies below the 4_1^+ state, reaching a minimum value of $E_s/E(2_1^+) = -0.67$ at the extreme triaxiality of $\gamma = 30°$.

Nuclei with negative $E_s/E(2_1^+)$ values between these two limits, 0 and −0.67, are typically characterized by γ-soft potential with a shallow minimum given by $\gamma \approx 30°$. In contrast, the positive value of $E_s/E(2_1^+)$ observed in $^{126-128}$Ba suggests an axially symmetric shape, as their ground states are prolate and the 2_2^+ state lies at a relatively high excitation energy compared to the 2_1^+ and 4_1^+ states.

As shown in Fig. 1 (b), ^{132,134,136}Ba exhibit negative values of approximately −0.20, −0.38, and −0.38, respectively, all higher than the rigid triaxial rotor limit of −0.67. The smallest ratio, approximately−0.38 in ^{134,136}Ba, remains slightly above the empirical value of $E_s/E(2_1^+) \approx -0.5$, which characterizes critical-point nuclei with maximal γ softness between prolate and oblate shapes.

Nuclei in transitional regions often exhibit complex level structures and soft, non-rigid shapes. Direct measurement of certain quantities, such as the triaxial parameter γ, remains challenging. However, the energy ratio $R_{4/2} \equiv E_{4_1^+}/E_{2_1^+}$ serves as a reliable indicator of nuclear shape deformation and can be used to assess the validity of the axial symmetry assumption. Deformations, including axial deformations, γ-unstable shapes, and spherical shapes, are all descriptions derived from collective models and serve to characterize different nuclear configurations.

For example, the energy ratio $R_{4/2}$ is approximately 3.3 for a well-deformed axially symmetric rotor, 2.5 for a γ-unstable shape, and 2.0 for a spherical vibrator. These values correspond to the dynamical symmetry limit of $SU(3)$, $O(6)$, and $U(5)$, respectively, in the IBM. More precisely, these symmetries represent different limiting cases: $SU(3)$ for the axially deformed (axially symmetric) rotor, $O(6)$ for the γ-unstable shape, and $U(5)$ for the spherical vibrator. For the $E(5)$ symmetry, which describes a critical point symmetry between the spherical vibrator and γ-unstable shape, the ratio is $R_{4/2} \approx 2.2$. For the $X(5)$ symmetry, which is a critical point symmetry between the spherical vibrator and axially deformed states, it is approximately $R_{4/2} \approx 2.9$ [36, 37]. It was pointed out that the level energy ratios $R_{I/2}$ are related to $R_{4/2}$ [38]. Furthermore, a linear relation between $R_{I/2}$ and $R_{4/2}$ was established in [39]:

$$R_{I/2} = R_{4/2}\frac{I(I-2)}{8} - \frac{I(I-4)}{4}. \tag{5}$$

This relationship can be derived from the Mallmann plot [38], where $R_{I/2}$ is represented as a function of $R_{4/2}$. The linear relationship arises from the proportionality between certain quantities represented by similar triangles in the plot. This relation is universal, applying to a range of nuclear shapes, including rotational, γ-unstable, and vibrational shapes, as well as the $E(5)$ and $X(5)$ symmetries.

For even-even $^{126-136}$Ba, Fig. 2 (a) shows the linear relation between the energy ratios $R_{6/2}$ and $R_{4/2}$ for the five typical shapes or symmetry limits, comparing both theoretical and experimental values. The theoretical ratio is given by $R_{6/2} = 3R_{4/2} - 3$ according to Eq. (5), while the experimental ratio is defined as $R_{6/2} = E_{6^+}/E_{2^+}$. As depicted in Fig. 2 (a), the ratio of even-even $^{126-132}$Ba follows a trajectory from vibrational towards axially deformed shape, passing through an intermediate structure resembling a γ-unstable shape, as noted in Ref. [46]. The calculated $R_{6/2}$ values of these nuclei generally agree well with the corresponding experimental results, particularly for

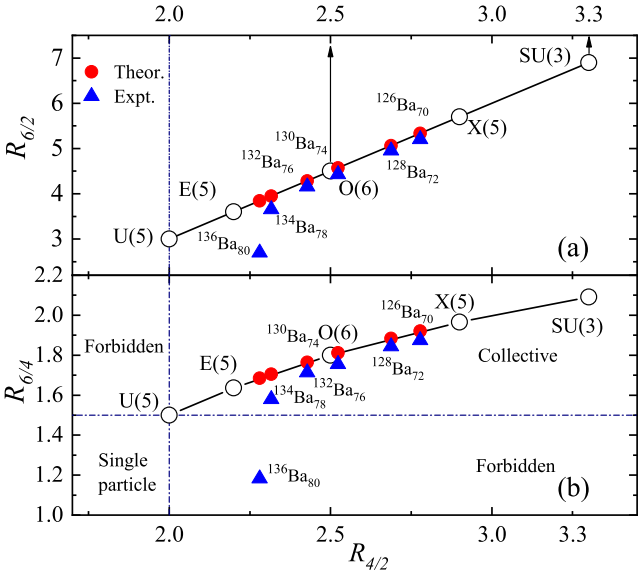

Fig. 2. (color online) (a) Linear plot of the energy ratio $R_{6/2}$ versus $R_{4/2}$ for five typical symmetries (empty circles), together with the calculated (solid circles) and experimental (solid triangles) values for comparison. (b) Similar energy ratio to that represented in (a) but for $R_{6/4}$ versus $R_{4/2}$. "Theor." represents theoretical values obtained using the empirical formula in Eq. (5), while the experimental data ("Expt.") were extracted from ^{126}Ba [40], ^{128}Ba [41], ^{130}Ba [42], ^{132}Ba [43], ^{134}Ba [44], and ^{136}Ba [45].

^{130}Ba, which is a typical example of $O(6)$ symmetry in the IBM, indicating the extreme γ-unstable limit, as shown in Fig. 1 (a).

From an analytical perspective, the experimental energy ratio $R_{6/2}$ for ^{134}Ba is 3.66, closely matching the theoretical $E(5)$ symmetry value of 3.95 with a deviation of approximately 7%. However, a more significant discrepancy between theoretical and experimental energy ratio values exists for ^{136}Ba. Notably, Cizewski *et al*. pointed out [47] that the energy ratio $R_{6/4}$ versus $R_{4/2}$ provides a more universally applicable description across nearly all collective nuclei (see Fig. 2 (b)). The ratio $R_{6/4}$ is less sensitive to variations in the moment of inertia, making it a more robust and less model-dependent parameter than $R_{6/2}$, particularly in transitional regions.

In Ref. [47], the onset of quadrupole collective motion is defined as $R_{4/2} = 2.0$, which corresponds to $R_{6/4} = 1.5$ in the collective model. The plot of $R_{6/4}$ versus $R_{4/2}$ divides the parameter space into four regions: single-particle, collective, and two forbidden regions. Nuclei with $R_{4/2} < 2.0$ and $R_{6/4} < 1.5$ are characterized by single-particle excitations, while those with $R_{4/2} \geq 2.0$ and $R_{6/4} \geq 1.5$ correspond to collective excitations. The two forbidden regions, in which $R_{4/2} > 2.0$ but $R_{6/4} < 1.5$, and $R_{4/2} < 2.0$ but $R_{6/4} > 1.5$, indicate conditions where the yrast structure does not align with either single-particle or collective excitation patterns.

Figure 2 (b) shows the energy ratio $R_{6/4}$ as a function of$R_{4/2}$, similar to Fig. 2 (a), with the calculated energy ratio given by $R_{6/4} = 3 - 3/R_{4/2}$ and the experimental energy ratio given by $R_{6/4} = E_{6^+}/E_{4^+}$. For even-even $^{126-136}$Ba, except for ^{136}Ba ($N = 80$), the experimental energy ratio of $R_{6/4}$ falls within the region where $R_{4/2} \geq 2$ and $R_{6/4} \geq 1.5$, which is characteristic of collective excitations. As noted by Cizewski *et al*. in [47], several $N = 80$ nuclei, such as ^{136}Ba, exhibit an energy ratio that falls into the forbidden region. The $R_{4/2}$ values of these nuclei shown in Fig. 2 (b) are all greater than 2.0, suggesting a collective, possibly non-axial structure, while the $R_{6/4}$ values point to a non-collective structure, typically associated with single-particle excitations. Given that the yrast energy ratios are influenced by the coexistence of collective and non-collective excitations, a spherical vibrator mode may provide a more suitable description for these nuclei. This is particularly relevant for nuclei near closed shells, where low-energy excitations are primarily governed by the motion of a few valence nucleons within spherical shell model orbitals. In contrast, as one moves away from shell closure, quadrupole collective excitations—ranging from vibrations near shell closure to rotations in mid-shell —become dominant. For isotopes $^{134-136}$Ba near the $N = 82$ shell, their relatively spherical shape suggests that their excitations can be described as a coupling between single-particle states and collective vibrational motion.

Figures 1−2 show that, as the neutron number increases from $N = 70$ to $N = 80$, the collective characteristic linked to quadrupole deformation gradually diminishes. Specifically, it is shown that ^{130}Ba lies at the γ-unstable point, while ^{136}Ba exhibits a non-collective structure. Given that nuclear rotational properties are shaped by the deformation and configuration of the ground state, it is interesting to explore the shapes that emerge from soft, γ-unstable, and non-collective configurations.

The above conclusions are based on phenomenological and empirical laws that describe nuclear deformation and low-energy states. To gain deeper insight into the microscopic mechanisms underlying these phenomena, we employed the TRS approach. This method allows comparing TRS results with previous experimental data based on collective models and the IBM as well as uncovering the microscopic origins of these experimental observations. By comparing TRS calculations with experimental results, we validated and refined predictions from collective models and the IBM, ultimately achieving a more comprehensive understanding of the nuclear structure. In the next section, we present TRS calculation results and their integration with experimental data and other theoretical frameworks, providing a more precise perspective on nuclear deformation and structural characteristics.

Within the framework of TRS calculations, the equilibrium deformation denoted by the black dot can be ex-

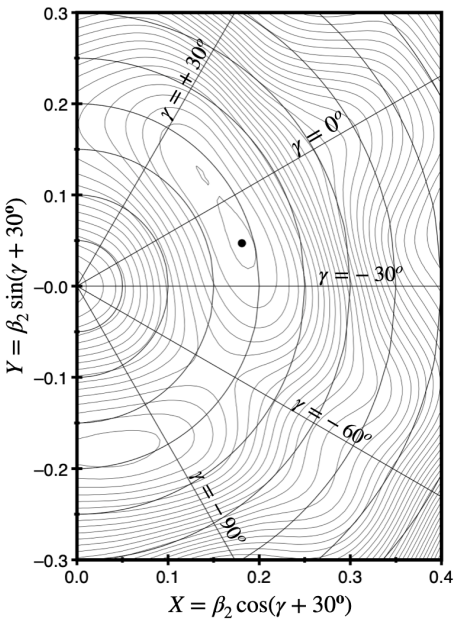

Fig. 3. Example of the potential energy surface projected on the Cartesian quadrupole coordinates for ^{130}Ba. The equilibrium deformation denoted by the black point is obtained by minimizing the TRS. The quadrupole deformation β_2 can be read from the circles; the typical γ deformations representing the prolate shape ($\gamma = 0°$ and $\gamma = -120°$), triaxial shape ($\gamma = \pm 30°$), and oblate shape ($\gamma = \pm 60°$) are marked.

tracted from the potential energy surface. As shown for the example of ^{130}Ba presented in Fig. 3, the equilibrium deformation at the ground state is approximately given by $\beta_2 = 0.184$, $\gamma = -10.5°$ $\beta_4 = -0.006$. The non-zero γ deformation indicates the flexibility of the shape in ^{130}Ba, which agrees with the empirical prediction of the γ-unstable shape shown in Fig. 1. Given that this nucleus is soft, the deformations and shapes may change easily. It is known that the dependence of the deformations can be studied by the single-particle level diagram qualitatively. In Fig. 4, we present the single-particle energy levels as functions of the quadrupole deformation β_2 and non-axil deformation γ.

Notably, in Fig. 4 (a), there are some differences compared to the standard modified harmonic-oscillator Nilsson diagram (see Ref. [48]). These differences can be attributed to the virtual crossings being preserved and the considerable γ deformation. The proton Fermi surface of $Z = 56$ lies in the lower part of the $h_{11/2}$ orbitals, favoring an elongate shape. In contrast, the gap of neutrons for $N = 74$ appears at $\gamma \approx \pm 15°$, which indicates the γ-soft deformation and agrees with the empirical results of the γ-unstable shape of ^{130}Ba shown in Figs. 1 and 2. Additionally, it occupies medium-to-high Ω orbitals of the $h_{11/2}$ subshell, which can lead to significant γ deformation or oblate deformation at $\gamma = \pm 60°$. It also exhibits a strong dependence on γ deformation compared to the lower-Ω orbitals. This behavior aligns with the well-established deformation-driving properties of spin-aligned unique parity orbitals [6, 49]. When the Fermi surface is near the bottom of the shell, prolate shapes or shapes with positive γ values are energetically favored. As the Fermi surface moves upward through the shell, collective triaxial deformation becomes prominent, and ultimately, near the top of the shell, an oblate shape is preferred.

In rapidly rotating nuclei, the Coriolis and centrifugal interactions can become sufficiently strong to alter nucleonic motion and disrupt superfluid (pairing) correlations and nuclear shape (mean field).

Figure 5 shows the evolution of the axial β_2 deformation, non-axial γ deformation, and hexadecapole β_4 deformation for even-even $^{126-136}$Ba isotopes. The well-deformed prolate shapes with $(\beta_2 \approx 0.25, \gamma \approx 0.0, \beta_4 \approx -0.011)$ and $(\beta_2 \approx 0.22, \gamma \approx 0.0, \beta_4 \approx -0.006)$ are presented in ^{126,128}Ba, which is consistent with the results reported in [36, 37]. The significant triaxial deformations

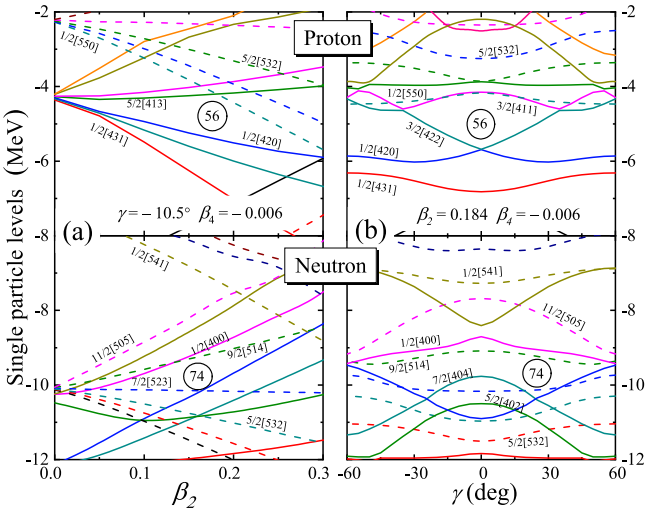

Fig. 4. (color online) (a) Single-particle levels calculated with a Woods-Saxon potential for ^{130}Ba as a function of β_2 for proton (upper) and neutron (lower) at $\gamma = -10.5°$ and $\beta_4 = -0.006$. The solid and dashed lines denote the positive and negative parity levels and are marked with the asymptotic labels $[Nn_z\Lambda]\Omega$. (b) Similar to (a): single-particle levels as a function of γ for proton (upper) and neutron (lower) for the ground state given by $\beta_2 = 0.184$ and $\beta_4 = -0.006$.

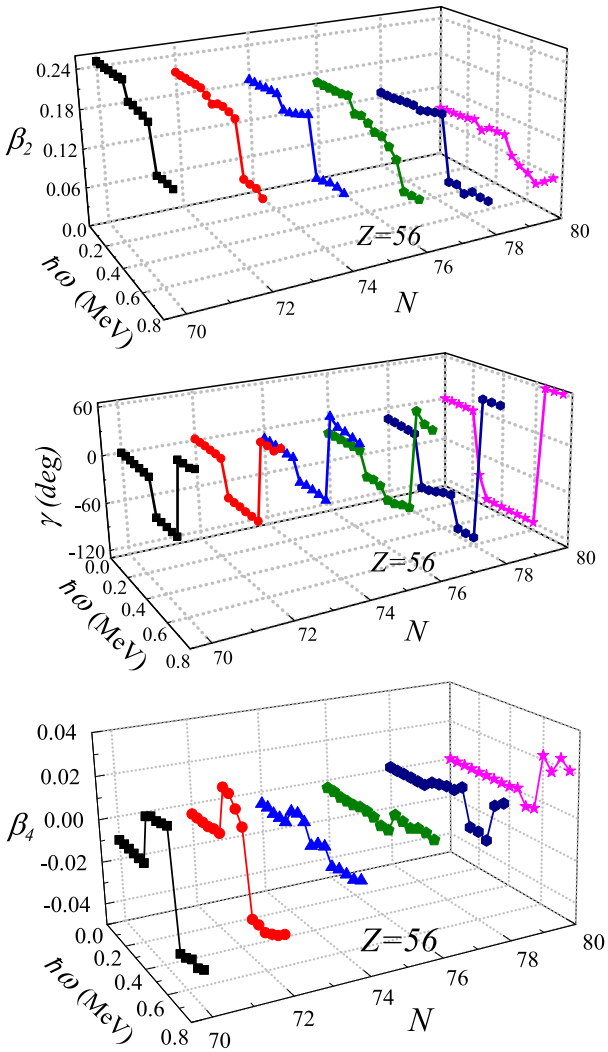

Fig. 5. (color online) Calculated deformation parameters β_2 (top), γ (middle), and β_4 (bottom) of yrast states for even-even $^{126-136}$Ba isotopes as a function of the rotational frequency $\hbar\omega$.

shown in Fig. 5(middle) are predicted for the ground states of $^{130-134}$Ba isotopes [42−45, 50, 51]. The ground-state deformations (β_2,γ,β_4) at $\hbar\omega = 0$ reveal systematic trends with increasing neutron number, which is consistent with experimental data shown in Fig. 1, and reflect the interplay between shell effects and deformation-driving interactions. The transitions in shape from prolate to γ-soft and then to spherical in isotopes $^{126-136}$Ba are consistent with the microscopic analysis performed using self-consistent relativistic mean-field theory combined with BCS calculations, as reported in Ref. [52]. Unstable γ deformations observed in isotopes ^{132}Ba and ^{134}Ba have been recognized as potential candidates for $E(5)$ behavior according to the self-consistent Hartree-Fock-Bogoliubov approximation [53]. Moreover,^{134}Ba has been studied as a promising candidate in Ref. [52] and in the self-consistent Relativistic Hartree Bogoliubov formalism reported in Ref. [54].

Recently, the impact of hexadecapole deformation has garnered attention in nuclear studies owing to its association with enhanced electric hexadecapole transitions and the low-energy $k^\pi = 4^+$ band cf. Ref. [55]. As shown in Fig. 5, the transition of hexadecapole β_4 deformations from negative to positive values corresponds to a change in shape from more prolate to more oblate, which agrees with the calculations presented in Refs. [49, 56].

The results shown in Figs. 4 and 5 demonstrate the feasibility and effectiveness of the TRS approach in describing the shape evolution of atomic nuclei. The consistency between TRS calculations and empirical observations shown in Figs. 1 and 2 confirms that the model can reliably capture both axial and triaxial deformation features across the Ba isotopic chain. The evolution of single-particle energy levels emphasizes the essential role of proton and neutron Fermi configurations in determining the preference for prolate, triaxial, or oblate shapes. The calculated deformation parameters (β_2,γ,β_4) reveal systematic trends with increasing neutron number, consistent with experimental data, and reflect the interplay between shell effects and deformation-driving forces. Therefore, the TRS approach is effective in describing nuclear shape evolution and provides a possible microscopic foundation under this model for the phenomena observed through phenomenological and empirical laws, shown in Figs. 1 and 2.

The equilibrium deformation is determined by minimizing the TRS at each rotational frequency, as shown in Fig. 3. With changes in the rotation frequency, the locations of the equilibrium deformations displayed on the potential energy surfaces in Fig. 3 may also shift. In Fig. 6, we present a schematic representation of the positions of the energy minima on the potential energy surface (PES) in the TRS for even-even $^{126-136}$Ba isotopes, with rotational frequency increasing from 0.0 to 0.80 MeV. The circles in the figure represent the positions of the energy minima corresponding to different values of rotational frequency. Each red circle in Fig. 6 represents an energy minimum corresponding to the black dot in Fig. 3, indicating the equilibrium deformation at different rotational frequencies.

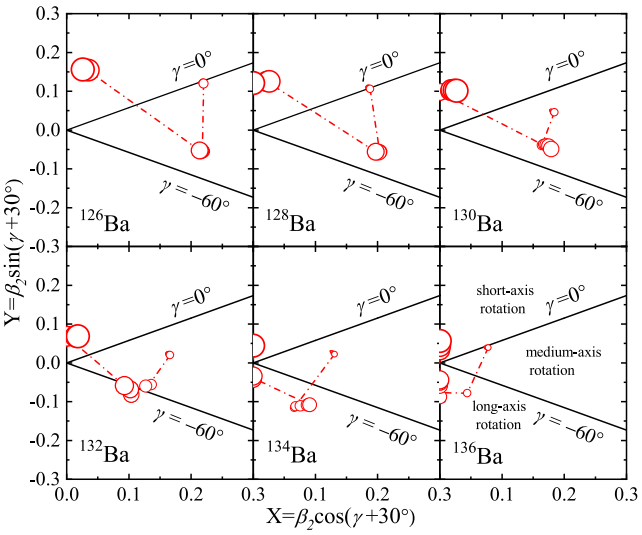

Fig. 6. (color online) Schematic representation of the positions of the energy minima in the TRS for even-even $^{126-136}$Ba isotopes. The gradually increasing circles represent the rotational frequency $\hbar\omega$ from 0.00 to 0.80 MeV. The γ range can be divided into three sectors, namely (−120°, −60°), (−60°, 0°), and (0°, 60°), which respectively represent rotation about the long, medium, and short axes, respectively.

As the rotational frequency increases, the positions of these minima shift, indicating the evolution of the nuclear shape and deformation. To visually capture this evolution, we created the schematic diagram shown in Fig. 6, where the varying sizes of the circles represent the changes in the minima locations as frequency increases. In the case of even-even $^{126-130}$Ba isotopes, the rotational axis evolves from intermediate-axis rotation ($-60° < \gamma < 0°$) to short-axis rotation ($0° < \gamma < 60°$) with increasing rotational frequency. For even-even $^{132-136}$Ba isotopes, the transition starts with intermediate-axis rotation and moves towards long-axis rotation ($-120° < \gamma < -60°$), ultimately shifting towards short-axis rotation as the frequency increases.

To explore the evolution of nuclear shape and the corresponding rotational axes, we present the calculated collective angular momenta for the even-even $^{126-136}$Ba nuclei in Fig. 7, including both proton and neutron components. As discussed previously, the even-even $^{126-136}$Ba nuclei exhibit a rotational axis transition from an intermediate-axis through a long-axis to a short-axis rotation with increasing rotational frequency.

The first substantial increase in total aligned angular momentum can be attributed to the neutron contribution. The rotational alignment of a pair of $h_{11/2}$ neutrons at

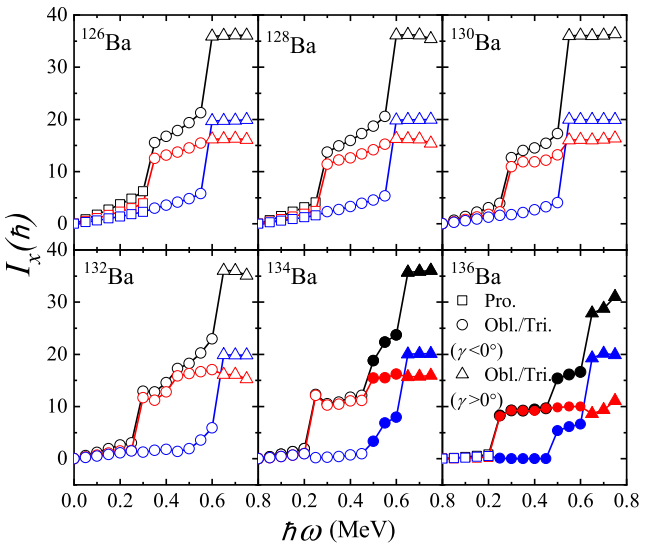

Fig. 7. (color online) Calculated aligned angular momenta (black symbols) as a function of rotational frequency $\hbar\omega$ for even-even $^{126-136}$Ba isotopes, together with the proton (blue symbols) and neutron (red symbols) components. The squares, circles, and triangles represent prolate (Pro.), oblate/triaxial (Obl./Tri.) ($\gamma < 0°$), and oblate/triaxial ($\gamma > 0°$) (the solid symbols denote non-collective mode), respectively.

$\hbar\omega \sim 0.3$ MeV is evident owing to the significant gain of approximately $10\hbar$. A second increase in rotational alignment appears to occur at a higher frequency, $\hbar\omega \sim 0.5$ MeV, where proton alignment becomes more favorable. This leads to distinct differences in the shape and rotational-axis driving tendencies between protons and neutrons. The proton and neutron $h_{11/2}$ configurations favor shapes with $\gamma > 0°$ (non-collective oblate/traxial) and $\gamma < 0°$ (collective oblate/triaxial), respectively [40–43, 50, 57].

Therefore, the alignments sensitively depend on the nuclear shape and rotational axis. The significant nuclear shape change associated with the alignment of the $(\nu h_{11/2})^2$ configuration may explain why the 10^+ bandhead of this two-quasineutron configuration was found to be isomeric, with measured mean lifetimes of $\tau = 12.5 \pm 0.3$ ns in ^{132}Ba [50] and 91 ± 2 ns in ^{136}Ba [45].

High-j nucleons occupying orbitals close to the Fermi surface are strongly influenced by the Coriolis interaction, which tends to align single-particle angular momenta along the rotation axis [58]. The ^{136}Ba nucleus lies near the neutron shell closure ($N = 82$) and in the proton mid-shell between the $Z = 50$ and 64 shell closures. In this region, an interplay between quadrupole collectivity and single-particle degrees of freedom can exist even in relatively low-lying states [57]. The $\nu(h_{11/2})^2$ configuration is expected to be dominant in the ^{134,136}Ba isotopes [57, 59], where the first neutron alignment drives the nuclear shape from triaxial/oblate towards non-collective prolate ($\gamma = -120°$) or non-collecitve oblate ($\gamma = +60°$). This evolution corresponds to the non-collective configuration predicted by the empirical laws shown in Fig. 2, while the TRS calculations provide a clear representation of the collective and non-collection shapes characterized by different γ values, as shown in Fig. 6.

The quasiparticle driving interaction competes with the restoring interaction of the core, which favors $\gamma = 0$ at $\hbar\omega = 0$. As ω increases, progressively negative γ values become energetically preferred owing to the irrotational flow behavior of collective rotation [60].

The shape-driving interactions (proportional to the slope in Fig. 8) are exerted by the quasiparticles, particularly the two-quasiproton and two-quasineutron configurations in the $h_{11/2}$ orbital. As shown in Fig. 8, the $(\nu h_{11/2})^2$ quasineutron configuration influences the evolution of the shape more strongly than the $(\pi h_{11/2})^2$ quasiproton configuration near the first rotational alignment frequency, as depicted in Fig. 8 (a). Consequently, γ values tend to cluster at $\gamma \sim -40°$, where oblate and triaxial shapes with negative γ dominate, as shown in Fig. 7.

At higher rotational frequencies, the behavior changes. The $(\pi h_{11/2})^2$ configuration exerts a strong driving interaction towards positive γ values near the second alignment frequency. Adding the $(\pi h_{11/2})^2$ pair may ultimately shift the nucleus towards a positive γ oblate/triaxial shape. This behavior is influenced by the Fermi surface configuration and the rotational alignment of nucleon pairs, which is crucial in dictating the transition from collective to non-collective excitations, as observed in these isotopes. The shift from prolate/triaxial to non-col-

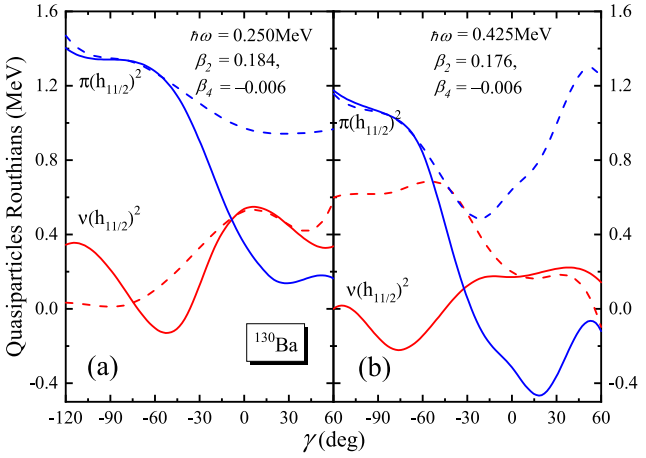

Fig. 8. (color online) (a) Calculated $(\pi h_{11/2})^2$ and $(\nu h_{11/2})^2$ quasiparticles Routhians as functions of triaxial deformation γ for ^{130}Ba at a given frequency (close to the first rotational alignment frequency) $\hbar\omega = 0.250$, $\beta_2 = 0.184$, and $\beta_4 = -0.006$. (b) Similar to (a), but for a given frequency (close to the second rotational alignment frequency) $\hbar\omega = 0.425$ at $\beta_2 = 0.176$ and $\beta_4 = -0.006$. The full line represents the positive signature states whereas the dashed line represents the negative signature partner band.

lective triaxial/oblate shape is a direct consequence of the interaction between the rotational motion and the underlying orbital structure.

Following the second rotational alignment, the collective band structure is lost, and the irregular yrast sequence of an oblate nucleus emerges, with single-particle angular momentum aligned along the short axis.

IV. CONCLUSIONS

In summary, phenomenological and empirical laws were applied in this study to explore the shape (phase) evolution in even-even $^{126-136}$Ba, for instance in terms of $E_S/E(2_1^+)$. This evolution serves as a global indicator of structural evolution involving axial asymmetry and the shape (phase) evolution from an axially symmetric shape to a γ-soft shape. The γ-unstable shape emerging in ^{130}Bawas verified by TRS calculations in terms of the Woods-Saxon single-particle energy levels as a function of β_2 and γ. This shape reveals that the medium-to-high Ω orbitals of a high-j shell are significantly affected by γ deformation. Moreover, the analysis of energy ratios ($R_{6/4}$ versus $R_{4/2}$) reveals the presence of both collective and non-collective excitations in ^{136}Ba ($N = 80$), suggesting that a spherical vibrator description may be more appropriate. This influences the non-collective configurations in high spin states, as demonstrated by the TRS calculations. These TRS calculations reproduce the observed trends and offer a possible microscopic foundation for phenomenological and empirical laws, elucidating how specific configurations of single-particle orbitals and nucleon alignments drive the shape evolution and phase transitions in $^{126-136}$Ba.

Additionally, TRS calculations for even-even $^{126-136}$Ba show the shape variations linked to the transition in rotational axes, progressing from intermediate-axis rotation to long-axis rotation, and finally to short-axis rotation as the frequency increases. These shape variations are driven by the rotational alignment of specific nucleon pairs at two critical frequencies. Near the first critical frequency ($\hbar\omega \sim 0.3$ MeV), the alignment of the $h_{11/2}$ neutron pair results in a significant negative γ deformation. At the second critical frequency ($\hbar\omega \sim 0.5$ MeV), positive γ deformation becomes more favorable owing to the rotational alignment of the $h_{11/2}$ proton pair.

These findings bridge the gap between empirical observations and microscopic nuclear structure, offering deeper insights into the mechanisms driving nuclear deformation and phase transitions.

References

[1] P. Ring, and P. Schunk, *The nuclear many-body problem* (Berlin: Springer-Verlag, 1980)
[2] G. Andersson, S. E. Larsson, G. Leander *et al*., Nucl. Phys. A **268**, 205 (1976)
[3] A. Bohr and B. R. Mottelson, *Nuclear structure. Vol. 1* (Singapore: World Scientific, 1975), p.197
[4] P. Möller, R. Bengtsson, B. G. Carlsson *et al*., Phys. Rev. Lett. **97**, 162502 (2006)
[5] R. F. Casten and P. V. Brentano, Phys. Lett. B **152**, 22 (1985)
[6] R. Wyss, A. Granderath, R. Bengtsson *et al*., Nucl. Phys. A **505**, 337 (1989)
[7] P. Olbratowski, J. Dobaczewski, J. Dudek *et al*., Phys. Rev. Lett. **93**, 052501 (2004)
[8] B. G. Carlsson, I. Ragnarsson, R. Bengtsson *et al*., Phys. Rev. C **78**, 034316 (2008)
[9] S. M. Burnett, A. M. Baxter, G. J. Gyapong *et al*., Nucl. Phys. A **494**, 102 (1989)
[10] F. Iachello and A. Arima, *The Interacting Boson Model*(Cambridge: Cambridge Univ. Press, 1987), p.188
[11] P. Petkov, A. Dewald, and W. Andrejtscheff, Phys. Rev. C **51**, 2511 (1995)
[12] Q. S. Zhang, Z. M. Niu, Z. P. Li *et al*., Front. Phys. **9**, 2529 (2014)
[13] B. X. Xiong, Phys. Rev. C **101**, 054305 (2020)
[14] L. Liu, Int. J. Mod. Phys. E **30**, 2150055 (2021)
[15] Z. H. Zhang, M. Huang, and A. V. Afanasjev, Phys. Rev. C **101**, 054303 (2020)
[16] Y. M. Wang and Q. B. Chen, Nucl. Sci. Tech. **35**, 183 (2024)
[17] Z. K. Li and Y. Y. Wang, Nucl. Sci. Tech. **35**, 189 (2024)
[18] H. L. Wang, J. Yang, M. L. Liu *et al*., Phys. Rev. C **92**, 024303 (2015)
[19] J. Yang, H. L. Wang, Q. Z. Chai *et al*., Prog. Theor. Exp. Phys. **6**, 063D03 (2016)
[20] W. Satuła, R. Wyss, and P. Magierski, Nucl. Phys. A **578**, 45 (1994)
[21] W. Satuła, and R. Wyss, Phys. Scr. **T56**, 159 (1995)
[22] F. R. Xu, W. Satuła, and R. Wyss, Nucl. Phys. A **669**, 119 (2000)
[23] W. D. Myers and W. J. Swiatecki, Nucl. Phys. **81**, 1 (1966)
[24] V. M. Strutinsky, Nucl. Phys. A **95**, 420 (1967)
[25] H. C. Pradhan, Y. Nogami, and J. Law, Nucl. Phys. A **201**, 357 (1973)
[26] S. Ćwiok, J. Dudek, W. Nazarewicz *et al*., Comp. Phys. Comm. **46**, 379 (1987)
[27] W. Greiner, and J. A. Maruhn, *Nuclear Models* (Berlin, Heidelberg: Springer- Verlag, 1996)
[28] W. Nazarewicz, J. Dudek, R. Bengtsson *et al*., Nucl. Phys. A **435**, 397 (1985)
[29] P. Cejnar, J. Jolie, and R. F. Casten, Rev. Mod. Phys. **82**, 2155 (2010)
[30] L. Grodzins, Phys. Lett. **2**, 88 (1962)
[31] F. S. Stephens, R. M. Diamond, J. R. Leigh *et al*., Phys. Rev. Lett. **29**, 438 (1972)
[32] B. Pritychenko, M. Birch, B. Singh *et al*., At. Data. Nucl. Data Tables **107**, 1 (2016)
[33] H. Watanabe, H. Yamaguchi, A. Odahara *et al*., Phys. Lett. B **704**, 270 (2011)
[34] L. Wilets and M. Jean, Phys. Rev. **102**, 788 (1956)
[35] A. S. Davydov and G. F. Filippov, Nucl. Phys. **8**, 237

(1958)
[36] F. Iachello, Phys. Rev. Lett. **85**, 3580 (2000)
[37] F. Iachello, Phys. Rev. Lett. **87**, 052502 (2001)
[38] C. A. Mallmann, Phys. Rev. Lett. **2**, 507 (1959)
[39] J. B. Gupta, Int. J. Mod. Phys. E **22**, 1350023 (2013)
[40] D. Ward, V. P. Janzen, H. R. Andrews *et al.*, Nucl. Phys. A **529**, 315 (1991)
[41] O. Vogel, R. S. Chakrawarthy, A. Dewald *et al.*, Eur. Phys. J. A **4**, 323 (1999)
[42] X. F. Sun, D. Bazzacco, W. Gast *et al.*, Phys. Rev. C **28**, 1167 (1983)
[43] S. Juutinen, S. Törmänen, P. Ahonen *et al.*, Phys. Rev. C **52**, 2946 (1995)
[44] U. S. National Nuclear Data Center http://www.nndc.bnl.gov/
[45] J. J. Valiente-Dobón, P. H. Regan, C. Wheldon *et al.*, Phys. Rev. C **69**, 024316 (2004)
[46] N. V. Zamfir, W. T. Chou, and R. F. Casten, Phys. Rev. C **57**, 427 (1998)
[47] J. A. Cizewski, Phys. Lett. B **219**(2), 189 (1989)
[48] T. Bengtsson and I. Ragnarsson, Nucl. Phys. A **436**(1), 14 (1985)
[49] A. Granderath, P. F. Mantica, R. Bengtsson *et al.*, Nucl. Phys. A **597**, 427 (1996)
[50] E. S. Paul, D. B. Fossan, Y. Liang *et al.*, Phys. Rev. C **40**, 1255 (1989)
[51] Q. Yang, H. L. Wang, Q. Z. Chai *et al.*, Chin. phys. C **39**(9), 094102 (2015)
[52] Z. P. Li, T. Nikšic, D.Vretenar *et al.*, Phys. Rev. C **81**, 034316 (2010)
[53] L. M. Robledo, R. R. Rodríguez-Guzmán, and P. Sarriguren, Phys. Rev. C **78**, 034314 (2008)
[54] T. Naz, G. H. Bhat, S. Jehangir *et al.*, Nucl. Phys. A **979**, 1 (2018)
[55] L. Lotina and K. Nomura, Phys. Rev. C **109**, 034304 (2024)
[56] M. Saha Sarkar and S. Sen, Phys. Rev. C **56**, 3140 (1997)
[57] T. Shizuma, Z. G. Gan, K. Ogawa *et al.*, Eur. Phys. J. A **20**, 207 (2004)
[58] J. L. Wood, K. Heyde, W. Nazarewicz *et al.*, Phys. Rep. **215**(), 101 (1992)
[59] P. Raghavan, At. Data Nucl. Data Tables **42**, 189 (1989)
[60] Y. S. Chen, S. Frauendorf, and L. L. Riedinger, Phys. Lett. B **171**, 7 (1986)